https://doi.org/10.1016/j.ymssp.2020.107563

To: Mechanical Systems and Signal Processing

Sparse Bayesian factor analysis for structural damage detection under unknown environmental conditions

Xiaoyou Wang
Department of Civil and Environmental Engineering,
The Hong Kong Polytechnic University,
Kowloon, Hong Kong, P. R. China
xiaoyou.wang@connect.polyu.hk

Lingfang Li
Department of Civil and Environmental Engineering,
The Hong Kong Polytechnic University,
Kowloon, Hong Kong, P. R. China
lingfang.li@connect.polyu.hk

James L. Beck
Division of Engineering and Applied Science,
California Institute of Technology,
Pasadena, CA, USA
jimbeck@caltech.edu

Yong Xia*
Department of Civil and Environmental Engineering,
The Hong Kong Polytechnic University,
Kowloon, Hong Kong, P. R. China
ceyxia@polyu.edu.hk

(* Corresponding author)

Sparse Bayesian factor analysis for structural damage detection under unknown environmental conditions

ABSTRACT

Damage detection of civil engineering structures needs to consider the effect of normal environmental variations on structural dynamic properties. This study develops a novel structural damage detection method using factor analysis in the sparse Bayesian learning framework. The unknown changing environmental factors that affect the structural dynamic properties are treated as latent variables in the model. The automatic relevance determination prior is adopted for the factor loading matrix for model selection. All variables and parameters, including the factor loading matrix, error vector and latent variables, are solved using the iterative expectation-maximization technique. The variables are then used to reconstruct structural responses. The Euclidean norm of the error vector is calculated as the damage indicator to detect possible damage when limited vibration data are available. Two laboratory-tested examples are utilized to verify the effectiveness of the proposed method. Results demonstrate that the number of underlying environmental factors and structural damage can be accurately identified, even though the changing environmental data are unavailable. The proposed method has the advantages of online monitoring and automatic identification of underlying environmental factors.

Keywords

Structural damage detection, sparse Bayesian learning, factor analysis, environmental variations, automatic relevance determination

1. Introduction

Vibration-based structural health monitoring (SHM) typically involves the long-term measurement of dynamic responses, followed by damage-sensitive feature extraction and structural condition assessment [1–5]. The principle behind vibration-based SHM is that damage causes variations in the structural dynamic properties, and so examining the variations may detect the damage via an inverse approach [1]. However, civil engineering structures are subject to ambient conditions, such as the temperature, humidity, wind and traffic loadings, that can vary significantly and also produce changes in structural dynamic properties [6–11]. If the changing environmental conditions are not fully considered, the emergence of structural damage may be masked, and false structural condition identification may occur [6, 8].

Various methods have been developed for structural damage detection under varying environmental conditions, particularly temperature. The methods can be classified into two kinds according to whether temperature is measured or not [12]. When temperature data are available, correlation models between the measured temperature and structural properties are established to explain the physical mechanism of the variations in structural dynamic properties [13–16]. Consequently the influence of temperature can be removed according to the fitted models. This kind of method is straightforward but relies heavily on the accurate and comprehensive measurement of environmental variables.

By comparison, the other category of methods conducts damage detection without measuring environmental factors. These methods learn the implicit relationship between temperature and vibration properties from the damage-sensitive features that are collected from the undamaged structure. The effect of damage that has not been captured in the undamaged state can then be distinguished from the effect of temperature. Representative techniques include auto-associative neural networks [17–

19], principal component analysis (PCA) [20–22], factor analysis (FA) [23–25], support vector machines [26], and Gaussian mixture models [27].

PCA is a widely used dimensionality reduction technique [20–22, 28–30] that uses a small subset of all of the principal components to account for most of the variance of the data. The measured structural responses collected before the structure experiences damage are used to compute the principal components. The data in the undamaged state can be reconstructed from several principal components with small errors, whereas the data in the damaged state cannot because the variations caused by damage have a different pattern from those induced by environment factors. Therefore, deviations in the reconstruction error will be observed with the emergence of damage. Representative approaches include the auto-associative neural network by Sohn et al. [17] that is essentially a nonlinear PCA, the linear and local nonlinear PCA methods by Yan et al. [21, 22] and the kernel PCA method by Reynders et al. [28]. However, the majority of these methods involve a tedious process because the number of principal components or dimensions to be retained is typically determined using a trial-and-error method, which is time-consuming, especially for high-dimensional problems.

Unlike PCA, which aims to find a linear combination of principal components to preserve the variance of data, FA provides a multi-variable statistical model in which factors are embedded as latent variables for interpreting changes in the measurement data [31]. An intuitive difference between the two techniques is that PCA treats the uncertainties of different components equally in the data reconstruction, whilst FA allows for a more comprehensive noise model that considers the uncertainty of each factor differently. Deraemaeker et al. [23, 24], Figueiredo et al. [19] and Kullaa [25] used FA for structural damage detection under changing environmental conditions. However, these studies restricted the covariance matrix to be diagonal, which implies that different modes are uncorrelated and independent. This assumption is questionable

because different vibration modes are generally extracted from the same set of time history data, and thus their uncertainties should be modeled as correlated. Additionally, it is desirable to automatically determine the number of environmental factors affecting structural dynamic properties, which is a challenging problem.

In recent decades, the Bayesian approach has been investigated for model selection [32–35] and uncertainty evaluation [5, 36–40]. Automatic relevance determination (ARD) and the highly-related sparse Bayesian learning (SBL) method are effective tools for pruning surplus or irrelevant features from the model and resulting in a sparse subset [41]. Tipping and Bishop [42, 43] developed a generative Bayesian PCA that incorporates the ARD prior. Latent dimensions of the data can be determined automatically due to the mechanism to induce sparseness. However, the covariance matrix in the Bayesian PCA was chosen as isotropic, so the matrix fails to model correlations between different modes. Inspired by the Bayesian PCA work, factor analysis in a sparse Bayesian framework is used in this study for structural damage detection. The proposed model adopts the same underlying structure as in Bayesian PCA but the covariance matrix is treated differently. A full covariance matrix is adopted to consider correlations between different modes. The ARD prior is adopted for the factor loading matrix in the FA model to automatically identify the number of latent environmental factors. The iterative expectation-maximization (EM) algorithm [31] is utilized to compute the maximum a posteriori (MAP) estimates of the FA model. Due to the nondiagonal covariance matrix, an analytical solution of the loading matrix is not directly available but it can be solved using the Sylvester equation via an optimization approach.

The rest of this paper is organised as follows. The sparse Bayesian framework of FA is presented in Section 2, followed by the EM algorithm which is used to compute all variables and parameters in Section 3. Section 4 summarizes the sparse Bayesian FA-

based method for structural damage detection. The application of the method to two experimental examples is presented in Section 5. Conclusions are drawn in Section 6.

2. FA in Sparse Bayesian Framework

FA was initially introduced by psychologists to identify the underlying factors accounting for correlations amongst a dataset of observations [44]. A statistical model is established to describe the variabilities of observations in terms of unobserved variables. Letting $\mathbf{D} = \left[\mathbf{D}_1, \mathbf{D}_{2,}, \ldots, \mathbf{D}_N\right] \in \mathbb{R}^{N_m \times N}$ be a set of N_m -dimensional predicted data vectors, the FA model is expressed as [31, 44]

$$\mathbf{D}_n = \mathbf{W}\mathbf{z}_n + \boldsymbol{\mu} + \boldsymbol{\varepsilon}_n \ (n = 1,2, \ldots, N) \tag{1}$$

where $\mathbf{W}$ is an $N_m \times M$ factor loading matrix, $\mathbf{z}_n$ is an M-dimensional standard Gaussian vector composed of M independent latent variables with prior density $\mathcal{N}(\mathbf{z}_n|\mathbf{0}, \mathbf{I})$, $\boldsymbol{\mu}$ is the global mean of vectors in $\mathbf{D}$, and $\boldsymbol{\varepsilon}_n$ is an N_m-dimensional error vector with prior Gaussian density $\mathcal{N}(\boldsymbol{\varepsilon}_n|\mathbf{0}, \boldsymbol{\Psi})$ that accounts for uncertain measurement and modelling errors. Conventional FA restricts the covariance matrix $\boldsymbol{\Psi} \in \mathbb{R}^{N_m \times N_m}$ to be diagonal, thereby modelling the elements in $\mathbf{D}_n$ as uncorrelated and independent.

FA is used for structural damage detection under unknown changing environmental conditions in this study. The training data comprises the evolution of natural frequencies in the undamaged state. Given that different modes in $\mathbf{D}_n \ (n = 1,2, \ldots, N)$ are correlated and dependent, the covariance matrix $\boldsymbol{\Psi}$ is chosen as a full matrix instead of a diagonal matrix to represent correlations between modes. Unknown environmental factors that affect structural frequencies correspond to $\mathbf{z}_n$. The calculation of the latent variable $\mathbf{z}_n$ and parameters $\mathbf{W}$, $\boldsymbol{\mu}$ and $\boldsymbol{\Psi}$ in Eq. (1) is a classical inverse problem from the data space to latent space, which can be solved using the Bayesian method.

The overall Bayesian equation to solve the latent variable $\mathbf{z} = [\mathbf{z}_1, \mathbf{z}_2, \dots, \mathbf{z}_N] \in \mathbb{R}^{M \times N}$ is expressed as [31]

$$p(\mathbf{z}|\mathbf{D}, \boldsymbol{\xi}) = c_0^{-1} p(\mathbf{D}|\mathbf{z}, \boldsymbol{\xi}) p(\mathbf{z}) \tag{2}$$

where $p(\mathbf{z}|\mathbf{D}, \boldsymbol{\xi})$ is the posterior probability density function (PDF) of the latent factor $\mathbf{z}$ given data $\mathbf{D}$ and model parameters $\boldsymbol{\xi} = \{\mathbf{W}, \boldsymbol{\mu}, \boldsymbol{\Psi}\}$, $p(\mathbf{D}|\mathbf{z}, \boldsymbol{\xi})$ is the likelihood function, $p(\mathbf{z})$ is the prior PDF of $\mathbf{z}$, $c_0 = \int p(\mathbf{D}|\mathbf{z}, \boldsymbol{\xi}) p(\mathbf{z}) d\mathbf{z} = p(\mathbf{D}|\boldsymbol{\xi})$ and $\mathbf{z}$ and $\boldsymbol{\xi}$ are chosen to be independent a priori. In Eq. (2), the actual observed data is substituted for $\mathbf{D}$, whereas Eq. (1) gives a predictive probabilistic model for what the data should be.

The posterior PDF of model parameters $\boldsymbol{\xi}$ is expressed as

$$p(\boldsymbol{\xi}|\mathbf{D}, \mathbf{z}) = c_1^{-1} p(\mathbf{D}, \mathbf{z}|\boldsymbol{\xi}) p(\boldsymbol{\xi}) \tag{3}$$

where $p(\mathbf{D}, \mathbf{z}|\boldsymbol{\xi})$ is the complete-data likelihood function, $p(\boldsymbol{\xi})$ is the prior of $\boldsymbol{\xi}$, and $c_1 = \int p(\mathbf{D}, \mathbf{z}|\boldsymbol{\xi}) p(\boldsymbol{\xi}) d\boldsymbol{\xi} = p(\mathbf{D}, \mathbf{z})$.

2.1 Prior PDF

As $\boldsymbol{\xi} = \{\mathbf{W}, \boldsymbol{\mu}, \boldsymbol{\Psi}\}$, $p(\boldsymbol{\xi})$ is expressed as $p(\boldsymbol{\xi}) = p(\mathbf{W}) p(\boldsymbol{\mu}) p(\boldsymbol{\Psi})$. As defined, $\mathbf{W}$ is an $N_m \times M$ matrix where M corresponds to the dimension of each latent variable. However, the value of M is unknown because the number of environmental factors is unavailable. To determine M, the ARD prior in Bayesian PCA [43] is adopted here for $\mathbf{W}$ for automatic model selection, that is, an independent Gaussian prior is defined over each column of $\mathbf{W}$ as follows

$$p(\mathbf{W}|\boldsymbol{\alpha}) = \prod_{i=1}^{M} \left(\frac{\alpha_i}{2\pi}\right)^{\frac{N_m}{2}} exp\left\{-\frac{1}{2} \alpha_i \mathbf{w}_i{}^{\mathrm{T}} \mathbf{w}_i\right\} \tag{4}$$

where the factor loading $\mathbf{w}_i$ is the ith column of $\mathbf{W}$, $\boldsymbol{\alpha} = [\alpha_1, \alpha_2, \dots, \alpha_M]^{\mathrm{T}}$ and α_i is

the hyper-parameter that governs the precision of $\mathbf{w}_i$. M is first assumed equal to N_m, making $\mathbf{W}$ an $N_m \times N_m$ matrix. In the optimization process shown in the next section, M will be optimized to a value corresponding to the number of environmental factors. For simplicity, non-informative priors are chosen for $\boldsymbol{\mu}$ and $\boldsymbol{\Psi}$. In Eq. (2), the prior $p(\mathbf{z})$ is defined to follow $\mathcal{N}(\mathbf{z}|\mathbf{0}, \mathbf{I})$, that is,

$$p(\mathbf{z}) = \prod_{n=1}^{N} p(\mathbf{z}_n) = \left(\frac{1}{2\pi}\right)^{\frac{MN}{2}} \prod_{n=1}^{N} exp\left\{-\frac{\mathbf{z}_n{}^{\mathrm{T}}\mathbf{z}_n}{2}\right\} \tag{5}$$

and $p(\mathbf{z}, \boldsymbol{\xi}) = p(\mathbf{z})p(\boldsymbol{\xi})$.

2.2 Observed-data Likelihood PDF

Using Eq. (1), the mean and covariance for the likelihood function $p(\mathbf{D}_n|\boldsymbol{\xi}, \mathbf{z}_n)$ are given by

$$\mathbb{E}[\mathbf{D}_n|\boldsymbol{\xi}, \mathbf{z}_n] = \mathbf{W}\mathbf{z}_n + \boldsymbol{\mu} + \mathbb{E}[\boldsymbol{\varepsilon}_n] = \mathbf{W}\mathbf{z}_n + \boldsymbol{\mu} \tag{6}$$

$$\mathrm{Cov}[\mathbf{D}_n|\boldsymbol{\xi}, \mathbf{z}_n] = \mathbb{E}[(\mathbf{D}_n - \mathbf{W}\mathbf{z}_n - \boldsymbol{\mu})(\mathbf{D}_n - \mathbf{W}\mathbf{z}_n - \boldsymbol{\mu})^{\mathrm{T}}] = \mathbb{E}[\boldsymbol{\varepsilon}_n\boldsymbol{\varepsilon}_n{}^{\mathrm{T}}] = \boldsymbol{\Psi} \tag{7}$$

Therefore $p(\mathbf{D}_n|\boldsymbol{\xi}, \mathbf{z}_n)$ follows the Gaussian distribution $\mathcal{N}(\mathbf{D}_n|\mathbf{W}\mathbf{z}_n + \boldsymbol{\mu}, \boldsymbol{\Psi})$. As $\boldsymbol{\varepsilon}_n(n = 1,2, \dots, N)$ are mutually independent, the observed-data likelihood function is given by

$$\begin{aligned} p(\mathbf{D}|\boldsymbol{\xi}, \mathbf{z}) &= \prod_{n=1}^{N} p(\mathbf{D}_n|\boldsymbol{\xi}, \mathbf{z}_n) \\ &= \left(\frac{1}{2\pi}\right)^{\frac{N_m N}{2}} |\boldsymbol{\Psi}|^{-\frac{N}{2}} \prod_{n=1}^{N} exp\left\{-\frac{1}{2}(\mathbf{D}_n - \mathbf{W}\mathbf{z}_n - \boldsymbol{\mu})^{\mathrm{T}}\boldsymbol{\Psi}^{-1}(\mathbf{D}_n - \mathbf{W}\mathbf{z}_n - \boldsymbol{\mu})\right\} \end{aligned} \tag{8}$$

where $|\boldsymbol{\Psi}|$ is the determinant of $\boldsymbol{\Psi}$.

2.3 Complete-data Likelihood PDF

Based on the assumption of prior independence of $\mathbf{z}$ and $\boldsymbol{\xi}$, the complete-data likelihood $p(\mathbf{D},\mathbf{z}|\boldsymbol{\xi})$ is a product of the observed-data likelihood function $p(\mathbf{D}|\boldsymbol{\xi},\mathbf{z})$ and the prior PDF $p(\mathbf{z})$ [31], that is

$$p(\mathbf{D},\mathbf{z}|\boldsymbol{\xi}) = p(\mathbf{D}|\boldsymbol{\xi},\mathbf{z})p(\mathbf{z}) \tag{9}$$

Substituting Eqs. (5) and (8) into Eq. (9), one has

$$\begin{aligned} &p(\mathbf{D},\mathbf{z}|\boldsymbol{\xi}) \\ &= \left(\frac{1}{2\pi}\right)^{\frac{(M+N_m)N}{2}} |\boldsymbol{\Psi}|^{-\frac{N}{2}} \prod_{n=1}^{N} exp\left\{-\frac{1}{2}(\mathbf{D}_n - \mathbf{W}\mathbf{z}_n - \boldsymbol{\mu})^{\mathrm{T}}\boldsymbol{\Psi}^{-1}(\mathbf{D}_n - \mathbf{W}\mathbf{z}_n - \boldsymbol{\mu}) - \frac{\mathbf{z}_n{}^{\mathrm{T}}\mathbf{z}_n}{2}\right\} \end{aligned} \tag{10}$$

2.4 Posterior PDF

Using Eq. (10), the posterior PDF of the latent variable $\mathbf{z}$ conditional on $\boldsymbol{\xi}$ is derived as

$$\begin{aligned} &p(\mathbf{z}|\mathbf{D},\boldsymbol{\xi}) = c_0^{-1}p(\mathbf{D}|\boldsymbol{\xi},\mathbf{z})p(\mathbf{z}) = c_0^{-1}p(\mathbf{D},\mathbf{z}|\boldsymbol{\xi}) \\ &\propto \prod_{n=1}^{N} exp\left\{-\frac{1}{2}(\mathbf{D}_n - \mathbf{W}\mathbf{z}_n - \boldsymbol{\mu})^{\mathrm{T}}\boldsymbol{\Psi}^{-1}(\mathbf{D}_n - \mathbf{W}\mathbf{z}_n - \boldsymbol{\mu}) - \frac{\mathbf{z}_n{}^{\mathrm{T}}\mathbf{z}_n}{2}\right\} \\ &\propto \prod_{n=1}^{N} exp\left\{\mathbf{z}_n{}^{\mathrm{T}}\mathbf{W}^{\mathrm{T}}\boldsymbol{\Psi}^{-1}(\mathbf{D}_n - \boldsymbol{\mu}) - \frac{1}{2}\mathbf{z}_n{}^{\mathrm{T}}(\mathbf{I} + \mathbf{W}^{\mathrm{T}}\boldsymbol{\Psi}^{-1}\mathbf{W})\mathbf{z}_n\right\} \end{aligned} \tag{11}$$

Since the PDF is quadratic in terms of $\mathbf{z}_n$, the posterior PDF of $\mathbf{z}$ follows a Gaussian distribution

$$p(\mathbf{z}|\mathbf{D},\boldsymbol{\xi}) = \prod_{n=1}^{N} \mathcal{N}(\mathbf{z}_n|\bar{\mathbf{z}}_n, \mathbf{C}_\mathbf{z}) \propto \prod_{n=1}^{N} exp\left\{-\frac{1}{2}(\mathbf{z}_n - \bar{\mathbf{z}}_n)^{\mathrm{T}}\mathbf{C}_\mathbf{z}{}^{-1}(\mathbf{z}_n - \bar{\mathbf{z}}_n)\right\} \tag{12}$$

$$\propto \prod_{n=1}^{N} exp\left\{\mathbf{z}_n{}^{\mathrm{T}}\mathbf{C}_{\mathbf{z}}{}^{-1}\bar{\mathbf{z}}_n - \frac{1}{2}\mathbf{z}_n{}^{\mathrm{T}}\mathbf{C}_{\mathbf{z}}{}^{-1}\mathbf{z}_n\right\}$$

By comparing Eqs. (11) and (12), the posterior covariance matrix and mean of $\mathbf{z}_n$ are seen to be

$$\mathbf{C}_{\mathbf{z}} = (\mathbf{I} + \mathbf{W}^{\mathrm{T}}\boldsymbol{\Psi}^{-1}\mathbf{W})^{-1} \in \mathbb{R}^{M\times M} \tag{13}$$

$$\bar{\mathbf{z}}_n = \mathbf{C}_{\mathbf{z}}\mathbf{W}^{\mathrm{T}}\boldsymbol{\Psi}^{-1}(\mathbf{D}_n - \boldsymbol{\mu}) \in \mathbb{R}^{M} \tag{14}$$

Note that the posterior covariance $\mathbf{C}_{\mathbf{z}}$ is independent of $\mathbf{D}_n$, whereas the posterior mean $\bar{\mathbf{z}}_n$ depends on $\mathbf{D}_n$. The MAP estimate of a Gaussian distribution is equal to the mean. Hence, the MAP of $\mathbf{z}_n$, denoted as $\hat{\mathbf{z}}_n$, is given by

$$\hat{\mathbf{z}}_n = \mathbb{E}_{\mathbf{z}}[\mathbf{z}_n|\mathbf{D}_n,\boldsymbol{\xi}] = \bar{\mathbf{z}}_n \tag{15}$$

The posterior second moment of $\mathbf{z}_n$ is given by

$$\mathbb{E}_{\mathbf{z}}[\mathbf{z}_n\mathbf{z}_n{}^{\mathrm{T}}|\mathbf{D}_n,\boldsymbol{\xi}] = \mathbf{C}_{\mathbf{z}} + \bar{\mathbf{z}}_n\bar{\mathbf{z}}_n^{\mathrm{T}} \tag{16}$$

Substituting Eqs. (4) and (10) into Eq. (3), the posterior PDF of model parameters $\boldsymbol{\xi} = \{\mathbf{W}, \boldsymbol{\mu}, \boldsymbol{\Psi}\}$ conditional on $\mathbf{z}$ and $\boldsymbol{\alpha}$ is derived as

$$\begin{aligned} p(\boldsymbol{\xi}|\mathbf{D},\mathbf{z},\boldsymbol{\alpha}) &= c_1^{-1}p(\mathbf{D},\mathbf{z}|\boldsymbol{\xi})p(\mathbf{W}|\boldsymbol{\alpha}) \\ &\propto \prod_{n=1}^{N} exp\left\{-\frac{1}{2}(\mathbf{D}_n - \mathbf{W}\mathbf{z}_n - \boldsymbol{\mu})^{\mathrm{T}}\boldsymbol{\Psi}^{-1}(\mathbf{D}_n - \mathbf{W}\mathbf{z}_n - \boldsymbol{\mu}) - \frac{\mathbf{z}_n{}^{\mathrm{T}}\mathbf{z}_n}{2}\right\} \\ &\quad \times \prod_{i=1}^{M} exp\left\{-\frac{1}{2}\alpha_i\mathbf{w}_i{}^{\mathrm{T}}\mathbf{w}_i\right\} \end{aligned} \tag{17}$$

where the unknown parameter vector $\boldsymbol{\alpha} = [\alpha_1, \alpha_2, \dots, \alpha_M]^{\mathrm{T}}$ needs to be estimated. The MAP estimate of parameters $\boldsymbol{\xi} = \{\mathbf{W}, \boldsymbol{\mu}, \boldsymbol{\Psi}\}$ cannot be directly obtained from Eq. (17) but can be calculated using the EM algorithm as shown in the next section.

3. EM Algorithm

The EM algorithm is a general technique that can be applied to find the maximum likelihood solutions of Bayesian models with latent variables [31]. It alternates between two updates named the expectation (E) and maximization (M) steps. The E step calculates the expectation of the logarithm of the complete-data likelihood function with respect to the latent variable, followed by the M step that maximizes this expectation with respect to the parameters. The successive E and M steps result in convergence to the maximum likelihood solutions of the parameters. In this study, the EM algorithm is used to obtain the MAP estimates of the Bayesian FA model with the defined prior over $\mathbf{W}$. The E step is still calculated using the complete-data likelihood function, while now the M step maximizes the sum of the expectation in the E step and the prior [31]. Detailed procedures are described as follows. We note that the expectation with respect to $\mathbf{z}$ is the posterior one throughout this section.

In the E step, the expectation with respect to $\mathbf{z}$ of the logarithm of the complete-data likelihood function is calculated using Eq. (10):

$$
\begin{aligned}
&\mathbb{E}_{\mathbf{z}}[\ln p\,(\mathbf{D},\mathbf{z}|\boldsymbol{\xi})] \\
&= \frac{(M+N_m)N}{2}\ln\left(\frac{1}{2\pi}\right) - \frac{N}{2}\ln|\boldsymbol{\Psi}| \\
&\quad + \sum_{n=1}^{N}\mathbb{E}_{\mathbf{z}}\left[-\frac{1}{2}(\mathbf{D}_n - \mathbf{W}\mathbf{z}_n - \boldsymbol{\mu})^{\mathrm{T}}\boldsymbol{\Psi}^{-1}(\mathbf{D}_n - \mathbf{W}\mathbf{z}_n - \boldsymbol{\mu}) - \frac{\mathbf{z}_n{}^{\mathrm{T}}\mathbf{z}_n}{2}\right] \qquad (18) \\
&= \frac{(M+N_m)N}{2}\ln\left(\frac{1}{2\pi}\right) - \frac{N}{2}\ln|\boldsymbol{\Psi}| - \sum_{n=1}^{N}\left[\frac{1}{2}(\mathbf{D}_n - \boldsymbol{\mu})^{\mathrm{T}}\boldsymbol{\Psi}^{-1}(\mathbf{D}_n - \boldsymbol{\mu})\right] \\
&\quad + \sum_{n=1}^{N}\left[(\mathbf{D}_n - \boldsymbol{\mu})^{\mathrm{T}}\boldsymbol{\Psi}^{-1}\mathbf{W}\mathbb{E}_{\mathbf{z}}[\mathbf{z}_n] - \frac{1}{2}\mathbb{E}_{\mathbf{z}}(\mathbf{z}_n{}^{\mathrm{T}}\mathbf{W}^{\mathrm{T}}\boldsymbol{\Psi}^{-1}\mathbf{W}\mathbf{z}_n)\right] - \sum_{n=1}^{N}\frac{1}{2}\mathbb{E}_{\mathbf{z}}(\mathbf{z}_n{}^{\mathrm{T}}\mathbf{z}_n)
\end{aligned}
$$

The M step involves the maximization of the sum of this expectation and the logarithm

of the prior on $\mathbf{W}$ with respect to $\boldsymbol{\xi}$ keeping $\boldsymbol{\alpha}$ fixed:

$$\begin{aligned} J(\boldsymbol{\xi}) &= \mathbb{E}_{\mathbf{z}}[\ln p\,(\mathbf{D},\mathbf{z}|\boldsymbol{\xi})] + \ln p\,(\mathbf{W}|\boldsymbol{\alpha}) \\ &= \frac{(M+N_m)N}{2}\ln\left(\frac{1}{2\pi}\right) - \frac{N}{2}\ln|\boldsymbol{\Psi}| - \sum_{n=1}^{N}\left[\frac{1}{2}(\mathbf{D}_n-\boldsymbol{\mu})^{\mathrm{T}}\boldsymbol{\Psi}^{-1}(\mathbf{D}_n-\boldsymbol{\mu})\right] \\ &\quad + \sum_{n=1}^{N}\left[(\mathbf{D}_n-\boldsymbol{\mu})^{\mathrm{T}}\boldsymbol{\Psi}^{-1}\mathbf{W}\mathbb{E}_{\mathbf{z}}[\mathbf{z}_n] - \frac{1}{2}\mathbb{E}_{\mathbf{z}}(\mathbf{z}_n{}^{\mathrm{T}}\mathbf{W}^{\mathrm{T}}\boldsymbol{\Psi}^{-1}\mathbf{W}\mathbf{z}_n)\right] \\ &\quad - \sum_{n=1}^{N}\frac{1}{2}\mathbb{E}_{\mathbf{z}}(\mathbf{z}_n{}^{\mathrm{T}}\mathbf{z}_n) + \frac{N_m M}{2}\ln\left(\frac{\alpha_i}{2\pi}\right) - \sum_{n=1}^{M}\left(\frac{1}{2}\alpha_i\mathbf{w}_i{}^{\mathrm{T}}\mathbf{w}_i\right) \end{aligned} \tag{19}$$

Setting the derivative of $J(\boldsymbol{\xi})$ with respect to $\mathbf{W}$, $\boldsymbol{\mu}$ and $\boldsymbol{\Psi}^{-1}$ separately to zero, respectively, we have

$$\frac{\partial J}{\partial \mathbf{W}} = \sum_{n=1}^{N}\boldsymbol{\Psi}^{-1}(\mathbf{D}_n-\boldsymbol{\mu})\mathbb{E}_{\mathbf{z}}[\mathbf{z}_n]^{\mathrm{T}} - \sum_{n=1}^{N}\boldsymbol{\Psi}^{-1}\mathbf{W}\mathbb{E}_{\mathbf{z}}[\mathbf{z}_n\mathbf{z}_n{}^{\mathrm{T}}] - \mathbf{W}\mathrm{diag}(\alpha_i) = 0 \tag{20}$$

$$\begin{aligned} \frac{\partial J}{\partial \boldsymbol{\Psi}^{-1}} &= \frac{1}{2}\sum_{n=1}^{N}[\boldsymbol{\Psi} - (\mathbf{D}_n-\boldsymbol{\mu})(\mathbf{D}_n-\boldsymbol{\mu})^{\mathrm{T}}] \\ &\quad + \sum_{n=1}^{N}(\mathbf{D}_n-\boldsymbol{\mu})\mathbb{E}_{\mathbf{z}}[\mathbf{z}_n]^{\mathrm{T}}\mathbf{W}^{\mathrm{T}} - \frac{1}{2}\sum_{n=1}^{N}\mathbf{W}\mathbb{E}_{\mathbf{z}}[\mathbf{z}_n\mathbf{z}_n{}^{\mathrm{T}}]\mathbf{W}^{\mathrm{T}} = 0 \end{aligned} \tag{21}$$

$$\frac{\partial J}{\partial \boldsymbol{\mu}} = -\sum_{n=1}^{N}[\boldsymbol{\Psi}^{-1}\boldsymbol{\mu} - \boldsymbol{\Psi}^{-1}\mathbf{D}_n] - \sum_{n=1}^{N}\boldsymbol{\Psi}^{-1}\mathbf{W}\mathbb{E}_{\mathbf{z}}[\mathbf{z}_n] = 0 \tag{22}$$

In the Bayesian PCA developed by Bishop [43], $\boldsymbol{\Psi}$ is assumed to be an isotropic diagonal matrix $\boldsymbol{\Psi} = \beta\mathbf{I}$. Thus, an analytical solution of $\mathbf{W}$ can be directly obtained using Eq. (20). However, the non-diagonal and non-isotropic assumption for $\boldsymbol{\Psi}$ in this study makes an analytical solution for $\mathbf{W}$ unavailable. In this regard, Eq. (20) is transformed into a Sylvester equation that is expressed as

$$\mathbf{A}\widehat{\mathbf{W}} + \widehat{\mathbf{W}}\mathbf{B} = \mathbf{C} \tag{23}$$

where $\mathbf{A} = \boldsymbol{\Psi}^{-1}$, $\mathbf{B} = \mathrm{diag}(\alpha_i)(\sum_{n=1}^{N}\mathbb{E}_{\mathbf{z}}[\mathbf{z}_n\mathbf{z}_n{}^{\mathrm{T}}])^{-1}$ and $\mathbf{C} = \boldsymbol{\Psi}^{-1}(\sum_{n=1}^{N}(\mathbf{D}_n - \boldsymbol{\mu})\mathbb{E}_{\mathbf{z}}[\mathbf{z}_n]^{\mathrm{T}})(\sum_{n=1}^{N}\mathbb{E}_{\mathbf{z}}[\mathbf{z}_n\mathbf{z}_n{}^{\mathrm{T}}])^{-1}$. The MAP value $\widehat{\mathbf{W}}$ is then solved using the Sylvester

function in MATLAB.

The MAP values of parameters $\boldsymbol{\mu}$ and $\boldsymbol{\Psi}$ are derived from Eq. (21) and (22), respectively, as

$$\widehat{\boldsymbol{\Psi}} = \frac{1}{N}\sum_{n=1}^{N}\{(\mathbf{D}_n - \boldsymbol{\mu})(\mathbf{D}_n - \boldsymbol{\mu})^{\mathrm{T}} - 2(\mathbf{D}_n - \boldsymbol{\mu})\mathbb{E}_{\mathbf{z}}[\mathbf{z}_n]^{\mathrm{T}}\mathbf{W}^{\mathrm{T}} + \mathbf{W}\mathbb{E}_{\mathbf{z}}[\mathbf{z}_n\mathbf{z}_n{}^{\mathrm{T}}]\mathbf{W}^{\mathrm{T}}\} \quad (24)$$

$$\widehat{\boldsymbol{\mu}} = \frac{1}{N}\sum_{n=1}^{N}\mathbf{D}_n \quad (25)$$

Eq. (25) is derived by substituting Eq. (14) into (22). $\mathbb{E}_{\mathbf{z}}[\mathbf{z}_n]$ and $\mathbb{E}_{\mathbf{z}}[\mathbf{z}_n\mathbf{z}_n{}^{\mathrm{T}}]$ in Eqs. (23)–(25) are the posterior estimates that are calculated from Eq. (15) and (16).

The negative second derivative of $J(\boldsymbol{\xi})$ with respect to $\boldsymbol{\xi}$, namely, the Hessian matrix, should be positive definite to ensure that $J(\boldsymbol{\xi})$ at the stationary points $\mathbf{W} = \widehat{\mathbf{W}}$, $\boldsymbol{\Psi} = \widehat{\boldsymbol{\Psi}}$ and $\boldsymbol{\mu} = \widehat{\boldsymbol{\mu}}$ is a local maximum, not a minimum or a saddle point. As defined, $\mathbf{W} \in \mathbb{R}^{N_m \times M}$, $\boldsymbol{\Psi} \in \mathbb{R}^{N_m \times N_m}$ and $\boldsymbol{\mu} \in \mathbb{R}^{N_m}$. Therefore, the Hessian matrix $\mathbf{H} \in \mathbb{R}^{(N_m \cdot M + N_m \cdot N_m + N_m)\times(N_m \cdot M + N_m \cdot N_m + N_m)}$. However, the explicit form of $\mathbf{H}$ is unavailable due to the high dimension and complicated elements in $\mathbf{H}$. In this study, the Symbolic Math Toolbox in MATLAB is employed to calculate the analytical expression of each element in $\mathbf{H}$. In the experimental examples, the numerical values of $\widehat{\mathbf{W}}$, $\widehat{\boldsymbol{\Psi}}$ and $\widehat{\boldsymbol{\mu}}$ obtained in each iteration are substituted into these elements of $\mathbf{H}$, and then its positive definiteness is examined by numerically computing its eigenvalues.

Choosing a non-informative priori for $\boldsymbol{\alpha}$, the MAP estimate of the hyper-parameter $\boldsymbol{\alpha}$ is given by

$$\begin{aligned}\widehat{\boldsymbol{\alpha}} &= \underset{\boldsymbol{\alpha}}{argmax}\, p(\boldsymbol{\alpha}|\mathbf{D}, \boldsymbol{\mu}, \boldsymbol{\Psi}) = \underset{\boldsymbol{\alpha}}{argmax}\, p(\mathbf{D}|\boldsymbol{\mu}, \boldsymbol{\Psi}, \boldsymbol{\alpha}) \\ &= \underset{\boldsymbol{\alpha}}{argmax} \int p(\mathbf{D}|\mathbf{W}, \boldsymbol{\mu}, \boldsymbol{\Psi}) p(\mathbf{W}|\boldsymbol{\alpha}) d\mathbf{W}\end{aligned} \quad (26)$$

However, a closed-form solution of the integral in Eq. (26) is intractable. The Laplace approximation is a technique that can be applied to solve the closed-form solution of the integral [45–47]. Assuming that the distribution $p(\mathbf{D}|\mathbf{W},\boldsymbol{\mu},\boldsymbol{\Psi})$ has a unique peak at $\widehat{\mathbf{W}}$, the asymptotic solution of the integral is obtained as [48]

$$\ln p\left(\mathbf{D}|\boldsymbol{\mu},\boldsymbol{\Psi},\boldsymbol{\alpha}\right) = \ln p\left(\mathbf{D}|\widehat{\mathbf{W}},\boldsymbol{\mu},\boldsymbol{\Psi}\right) + \ln p\left(\widehat{\mathbf{W}}|\boldsymbol{\alpha}\right) + \frac{N}{2}\ln(2\pi) - \frac{1}{2}\ln|\mathbf{P}| \tag{27}$$

where $\widehat{\mathbf{W}}$ is the MAP estimate of $\mathbf{W}$ calculated from Eq. (23), and $\mathbf{P}$ is the Hessian matrix expressed as

$$\mathbf{P} = -\nabla\nabla \ln p\left(\mathbf{D}|\widehat{\mathbf{W}},\boldsymbol{\mu},\boldsymbol{\Psi}\right)p\left(\widehat{\mathbf{W}}|\boldsymbol{\alpha}\right) \tag{28}$$

From Eq. (27), setting the derivative of $\ln p\left(\mathbf{D}|\boldsymbol{\mu},\boldsymbol{\Psi},\boldsymbol{\alpha}\right)$ with respect to $\boldsymbol{\alpha}$ to zero, one has

$$\hat{\alpha}_i = \frac{N_m}{\mathbf{w}_i{}^{\mathrm{T}}\mathbf{w}_i + [\mathbf{P}^{-1}]_{ii}} \tag{29}$$

Bishop [43] treated all parameters as well-determined to simplify the solution further as

$$\hat{\alpha}_i = \frac{N_m}{\mathbf{w}_i{}^{\mathrm{T}}\mathbf{w}_i} \tag{30}$$

The solutions to the MAP values of the latent variables, parameters and hyper-parameter in Eqs. (15), (23)–(25) and (30) are coupled and thus must be calculated iteratively. The algorithm starts by initializing the parameters and then calculating the statistics of the latent variable using Eqs. (15) and (16), and then alternatively updating the parameters using Eqs. (23)–(25) and hyper-parameters via Eq. (30). The number of latent factors is first assumed equal to the dimensionality N_m of the data sample and $\mathbf{W}$ is then initialized as an $N_m \times N_m$ matrix. During the optimization process, some of α_i will approach infinity, automatically enforcing the factor loading $\mathbf{w}_i$ and the corresponding latent factors to zero. The corresponding zero column $\mathbf{w}_i$ is then

removed in the iterative process to ensure a unique solution of the Sylvester equation in Eq. (23). Upon convergence, the optimal $\mathbf{W}$ is an $N_m \times M$ matrix, where M corresponds to the number of latent factors. In this manner, the number of environmental factors affecting structural vibration properties is automatically determined.

4. Summary of Sparse Bayesian FA-based Method

The procedure of the proposed method is summarized as follows:

---

1. Extract structural dynamic properties collected in the undamaged state as the training data from the entire dataset $\mathbf{D}$;
2. Let $M = N_m$ first, initialize $\mathbf{W}^{(0)}$ and $\mathbf{\Psi}^{(0)}$, and calculate the mean $\boldsymbol{\mu}$ of the training data using Eq. (25);
3. Use the training data to calculate unknown variables and parameters. At the *j*th iteration
   (1) Let M equal the number of nonzero columns in $\mathbf{W}^{(j-1)}$. Update $\mathbf{W}^{(j-1)}$ as an $N_m \times M$ matrix by removing the zero columns $\mathbf{w}_i$.
   (2) Given $\mathbf{W}^{(j-1)}$, $\mathbf{\Psi}^{(j-1)}$ and $\boldsymbol{\mu}$:
   Update $\mathbb{E}_{\mathbf{z}}[\mathbf{z}_n]^{(j)}$ and $\mathbb{E}_{\mathbf{z}}[\mathbf{z}_n \mathbf{z}_n{}^{\mathrm{T}}]^{(j)}$ using Eqs. (15) and (16);
   Update $\boldsymbol{\alpha}^{(j)}$ using Eq. (30);
   (3) Update $\mathbf{W}^{(j)}$ and $\mathbf{\Psi}^{(j)}$ using Eqs. (23) and (24), respectively;
4. Let $j = j + 1$, repeat Step 3 until the convergence criterion is satisfied, that is, $\left\|\mathbf{\Psi}^{(j)} - \mathbf{\Psi}^{(j-1)}\right\| / \left\|\mathbf{\Psi}^{(j)}\right\| \leq Tol$ (e.g. $Tol = 1{\times}10^{-5}$).
5. Based on the determined $\mathbf{W}$, $\boldsymbol{\mu}$ and $\mathbf{\Psi}$, calculate $\hat{\mathbf{z}}_n$ of the entire dataset $\mathbf{D}$ using Eq. (15), and then re-generate a new dataset $\mathbf{D}' = \mathbf{W}\hat{\mathbf{z}} + \boldsymbol{\mu} + \boldsymbol{\varepsilon}$.
6. Calculate the Euclidean norm of the error vector $\|\mathbf{e}\|_2 = \|\mathbf{D} - \mathbf{D}'\|_2$ as the damage indicator for structural condition evaluation.

The proposed method has the following advantages. First, the number of underlying environmental factors that affect structural dynamic properties is automatically determined using the ARD prior. Second, the method can be implemented in an online form with the EM algorithm, in which each data vector $\mathbf{D}_n$ can be processed individually and then discarded before the next data is read in [31].

5. Experimental Validation

Two experimental examples are presented in this section to illustrate the effectiveness of the proposed method. The first is a reinforced concrete (RC) slab for automatically determining the number of latent environmental factors, and the second is a steel frame for damage detection under varying environmental conditions.

5.1 RC slab

The RC slab [8] measures 6400 mm × 800 mm × 100 mm with two equal spans of 3000 mm and 200 mm at each end, as shown in Figure 1. The structure was monitored from June 2003 to March 2005. One hundred thirty-six sets of modal properties were collected. Although the corresponding temperature and humidity were measured, they are not used in this study. The first four frequencies versus sample number are illustrated in Figure 2.

Figure 1 RC slab

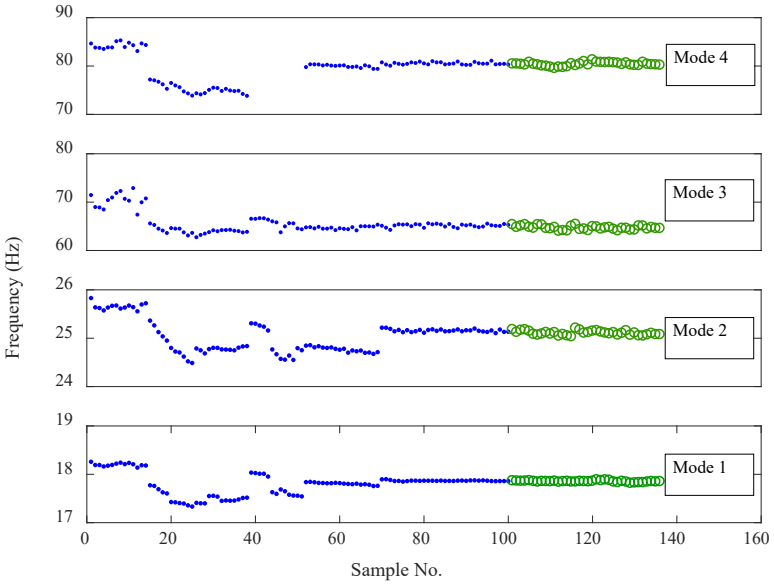

Figure 2 Variations of the first four frequencies of the RC slab

(Blue dots: training data (N=100); green circles: test data in the undamaged state)

Data of Nos. 39 ~51 of the fourth frequency were not identified in the test. The first 100 sets of data except the lost data are utilized for training. $\mathbf{W}$ and $\mathbf{\Psi}$ are initialized and the mean of the training data is calculated first. In this study, $\mathbf{W}^{(0)}$ is randomly generated from the uniform distribution in the interval (0, 1). $\mathbf{\Psi}$ stands for the covariance of the prediction error. It is initialized as a semi-positive definite matrix by assuming that the coefficient of variation of each modal frequency is 1% and the correlation coefficients of all modes are 0.5. $\mathbf{W}^{(0)}$ and $\mathbf{\Psi}^{(0)}$ are shown in Table 1. The convergence criterion of the iteration process is set to $\left\|\mathbf{\Psi}^{(j)}-\mathbf{\Psi}^{(j-1)}\right\| / \left\|\mathbf{\Psi}^{(j)}\right\| \leq 1\times10^{-5}$.

The EM process took fifteen iterations to converge with the proposed method. The evolution of parameters is listed in Table 1. The numerical values of $\mathbf{W}$, $\mathbf{\Psi}$ and $\boldsymbol{\mu}$ obtained in each iteration are substituted into the analytical expression of each element in the Hessian matrix computed using the Symbolic Math Toolbox in MATLAB. The Hessian matrix is found to have all positive eigenvalues and so be positive definite in

all iterations, indicating that the solutions of parameters in Eqs. (23)–(25) correspond to a local maximum of $J(\boldsymbol{\xi})$. As the process proceeds, two components of $\boldsymbol{\alpha}$ become larger and larger and approach infinity upon convergence. The corresponding two columns of $\mathbf{W}$ are then enforced to zero. Correspondingly, two components of $\mathbf{z}_n$ become zero. The remaining two nonzero components of $\mathbf{z}_n$ corresponding to latent factors reflect that variations of the first four frequencies can be represented by two environmental factors only. This finding is consistent with the results of Ref. [8] wherein the slab's frequencies have a strong correlation with environmental temperature and humidity. This example indicates that the sparse Bayesian FA-based method can automatically identify the number of significant environmental factors that influence structural dynamic properties. Another advantage of the present strategy is that the measurement of the two environmental factors is unnecessary. This is promising for practical applications because the latent variables are commonly unknown.

Table 1 Variation of the variable and parameters in the RC slab example

Iteration No.	$\boldsymbol{\alpha}$	$\mathbf{W}$	$\mathbf{z}_1$	M	$\boldsymbol{\Psi}$
0		$\begin{bmatrix} 0.19 & 0.44 & 0.58 & 0.18 \\ 0.04 & 0.43 & 0.59 & 0.29 \\ 0.60 & 0.75 & 0.17 & 0.71 \\ 0.96 & 0.43 & 0.81 & 0.26 \end{bmatrix}$		4	$\begin{bmatrix} 0.03 & 0.02 & 0.06 & 0.07 \\ 0.02 & 0.06 & 0.08 & 0.10 \\ 0.06 & 0.08 & 0.43 & 0.26 \\ 0.07 & 0.10 & 0.26 & 0.63 \end{bmatrix}$
1	$\begin{Bmatrix} 3.1 \\ 3.6 \\ 2.9 \\ 5.8 \end{Bmatrix}$	$\begin{bmatrix} 0.12 & 0.04 & 0.06 & 0.03 \\ 0.13 & 0.13 & 0.13 & 0.14 \\ 0.77 & 0.20 & -0.70 & 0.59 \\ 1.55 & -0.09 & 0.17 & 0.10 \end{bmatrix}$	$\begin{Bmatrix} 3.04 \\ 0.46 \\ -1.62 \\ 2.57 \end{Bmatrix}$	4	$\begin{bmatrix} 0.01 & 0.01 & 0.04 & 0.08 \\ 0.01 & 0.04 & 0.08 & 0.11 \\ 0.04 & 0.09 & 0.53 & 0.41 \\ 0.08 & 0.12 & 0.41 & 1.03 \end{bmatrix}$
8	$\begin{Bmatrix} \text{Inf} \\ 0.4 \\ 6.4 \\ 31.8 \end{Bmatrix}$	$\begin{bmatrix} 0.20 & 0.02 & 0.01 \\ 0.21 & 0.02 & 0.07 \\ 1.58 & -0.75 & 0.24 \\ 2.60 & 0.11 & -0.16 \end{bmatrix}$	$\begin{Bmatrix} 2.33 \\ 0.62 \\ 0.05 \end{Bmatrix}$	3	$\begin{bmatrix} 0.01 & 0.02 & 0.11 & 0.16 \\ 0.02 & 0.05 & 0.24 & 0.20 \\ 0.12 & 0.25 & 1.55 & 1.13 \\ 0.16 & 0.20 & 1.10 & 2.10 \end{bmatrix}$
15	$\begin{Bmatrix} \text{Inf} \\ 0.5 \\ 200 \\ \text{Inf} \end{Bmatrix}$	$\begin{bmatrix} 0.19 & 0.03 \\ 0.18 & 0.11 \\ 1.44 & -0.03 \\ 2.51 & 0.01 \end{bmatrix}$	$\begin{Bmatrix} 1.38 \\ 0.32 \end{Bmatrix}$	2	$\begin{bmatrix} 0.02 & 0.02 & 0.11 & 0.19 \\ 0.02 & 0.06 & 0.34 & 0.27 \\ 0.11 & 0.34 & 2.30 & 1.50 \\ 0.19 & 0.27 & 1.50 & 2.60 \end{bmatrix}$

Note: N=100 in this RC slab example, namely, there are 100 components in $\mathbf{z} = [\mathbf{z}_1, \mathbf{z}_2, \ldots, \mathbf{z}_N] \in \mathbb{R}^{M \times N}$. We only list the first component $\mathbf{z}_1$ here for demonstration due to the space limit. All of the 100 components in $\mathbf{z}$ are initialized to 4-dimensional vectors and converge to two-dimensional vectors in the 15th iteration.

Upon convergence, $\boldsymbol{\Psi}$ converges to a full matrix where each diagonal element represents the variance of each component of the prediction error, and each off-diagonal element is the covariance between different components, as shown in Table 1. The correlation coefficient between components i and j can be calculated as $\rho_{ij} = \frac{\boldsymbol{\Psi}_{ij}}{\sqrt{\boldsymbol{\Psi}_{ii}}\sqrt{\boldsymbol{\Psi}_{jj}}}$ (i, j =1, 2, 3, and 4). Using the determined $\mathbf{W}^{(15)}$ and $\boldsymbol{\Psi}^{(15)}$, we can calculate the MAP estimates of the latent variables according to Eq. (15) and then re-generate the dataset $\mathbf{D}'$ according to Eq. (1). The reconstruction error of the training and test data both corresponding to the undamaged state, is calculated as the damage indicator $\|\mathbf{e}\|_2 = \|\mathbf{D} - \mathbf{D}'\|_2$. The 2-norm of the error vector is plotted in Figure 3. The reconstruction error of the test data is comparable to that of the training data, indicating that the RC slab is in the undamaged state during the monitoring period.

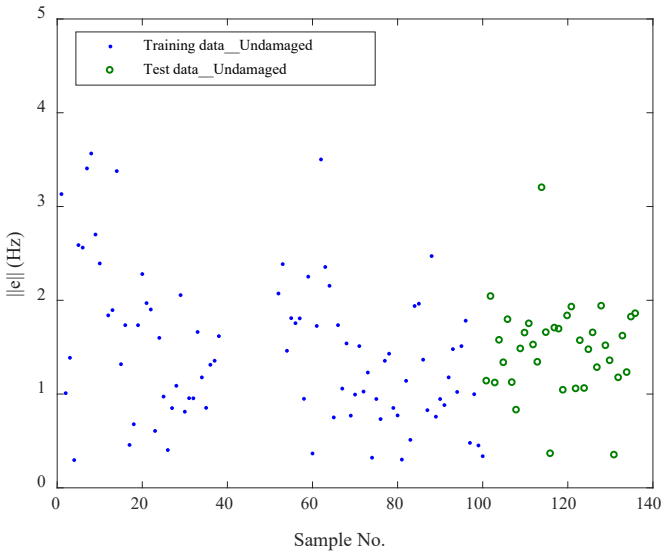

Figure 3 Reconstruction error of the training and test data of the RC slab

5.2 Steel frame

The two-storey steel frame in Bao et al. [14] is utilized in this study to demonstrate the

effectiveness of the proposed method for damage detection under varying environmental conditions. The structure is 0.5 m wide and 1.0 m high with two equal stories, as shown in Figure 4. The Young's modulus and mass density are 2.0×10^{11} N/m^2 and 7.67×10^3 kg/m^3, respectively. The intact frame was tested from morning to afternoon on August 27, 2010. Fourteen accelerometers were installed on columns and beams to collect vibration responses. A series of modal tests conducted on the frame resulted in 140 sets of modal data throughout the day.

Figure 4 Experimental steel frame

Damage was then introduced to the steel frame. A saw cut was located at the left column of the frame, as shown in Figure 5. The depth of the cut was set to 5, 10 and 15 mm in sequence with the identical length of 20 mm. Correspondingly, the moment of inertia of the cut section in these three damage scenarios (DSs) was reduced by 20%, 40% and 60%, respectively. The modal testing was similarly conducted on each damage scenario from morning to afternoon, and 140 sets of modal data of each DS were collected.

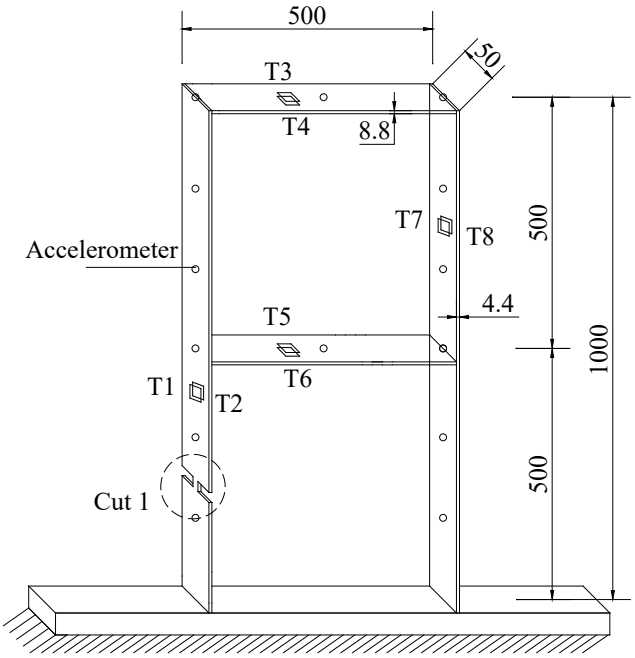

Figure 5 Configuration of the experimental frame and damage locations (unit: mm)

The first six frequencies of the steel frame under undamaged and damaged conditions are compared in Table 2. The values presented are the averages of the total 140 sets of frequencies in each DS. The intact frame is denoted DS0. DS1 caused an average frequency change of 0.26% only in average while DS2 and DS3 caused 0.64% and 0.79% average frequency reductions, respectively. Variations of the frequencies during the monitoring period are plotted in Figure 6. The temperature of the frame was also recorded [14], but it is assumed unknown in this study and only the frequency data are used for damage detection.

Table 2 Frequencies of the frame in undamaged and damaged states (unit: Hz)

Mode	DS0	DS1	DS2	DS3
1	6.20	6.19(−0.19)	6.17(−0.43)	6.19(−0.13)
2	17.57	17.49(−0.49)	17.48(−0.52)	17.45(−0.72)
3	61.07	60.97(−0.17)	60.83(−0.39)	60.74(−0.55)
4	77.01	76.97(−0.05)	76.65(−0.47)	76.32(−0.89)
5	80.83	80.73(−0.13)	80.16(−0.83)	80.05(−0.97)
6	98.09	97.58(−0.52)	96.91(−1.20)	96.66(−1.46)
Average (%)		(−0.26)	(−0.64)	(−0.79)

Note: Values in parentheses are the frequency change ratios (%) between the damaged and undamaged states.

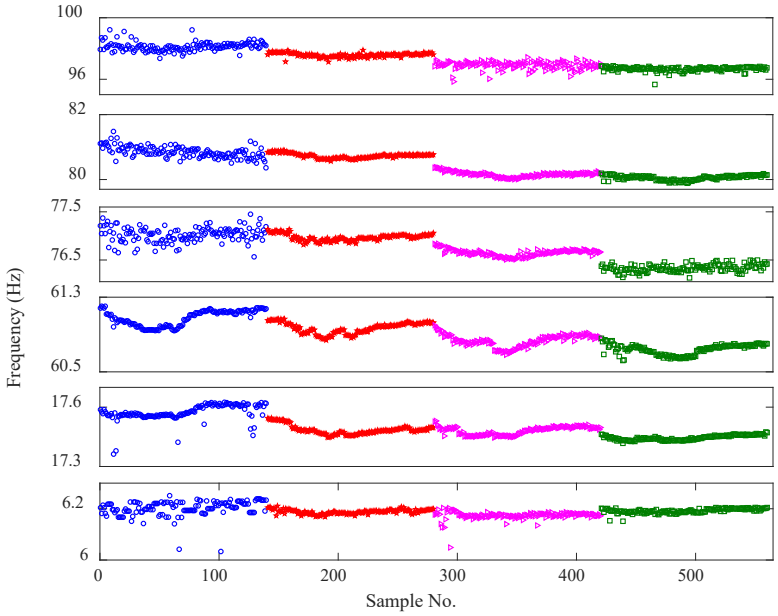

Figure 6 First six frequencies of the steel frame

(Blue circles: DS0; red pentagrams: DS1; carmine triangles: DS2; and green squares: DS3)

The proposed sparse Bayesian FA-based method is applied to the first six modes. One hundred and forty sets of the first six frequencies in the undamaged state are used as training data. $\mathbf{W}^{(0)}$ is again generated from the uniform distribution in (0, 1), and the initialization of $\mathbf{\Psi}^{(0)}$ is the same as that described in Section 5.1. Convergence is achieved after nine iterations. Table 3 lists the variations of parameters. The Hessian matrix $\mathbf{H}$ has all positive eigenvalues and so is positive definite in all iterations. Upon convergence, five components of $\boldsymbol{\alpha}$ approach to infinity, enforcing five columns of $\mathbf{W}$ to zero. Only one component of $\mathbf{z}_n$ remains nonzero, indicating that only one significant environmental factor is responsible for variations of the training data.

Simulated datasets for DS0–DS3 are reconstructed with the determined $\mathbf{W}^{(9)}$ and $\mathbf{\Psi}^{(9)}$. Reconstruction errors are then calculated and plotted in Figure 7. The damage-induced deviations can be observed from the figure. The deviation is relatively small but still recognizable when damage severity is slight (i.e. DS1). When damage

becomes severe (i.e. DS2 and DS3), the reconstruction error increases significantly. Therefore, the reconstruction error can be treated as a damage index that indicates that the steel frame in DS1–DS3 is in a damaged state.

Table 3 Variations of the variable and parameters in the steel frame example

No.	$\boldsymbol{\alpha}$	$\mathbf{W}$	$\mathbf{z}_1$	M	$\boldsymbol{\Psi}$
0		$\begin{bmatrix} 0.43 & 0.67 & 0.54 & 0.18 & 0.08 & 0.53 \\ 0.24 & 0.55 & 0.24 & 0.18 & 0.80 & 0.19 \\ 0.71 & 0.73 & 0.06 & 0.53 & 0.66 & 0.75 \\ 0.41 & 0.22 & 0.89 & 0.85 & 0.99 & 0.75 \\ 0.80 & 0.61 & 0.32 & 0.82 & 0.14 & 0.30 \\ 0.57 & 0.32 & 0.46 & 0.81 & 0.67 & 0.68 \end{bmatrix}$		6	$10^{-3}\times\begin{bmatrix} 4 & 5 & 19 & 24 & 25 & 30 \\ 5 & 31 & 54 & 68 & 71 & 86 \\ 19 & 54 & 373 & 235 & 247 & 300 \\ 24 & 68 & 235 & 593 & 311 & 378 \\ 25 & 71 & 247 & 311 & 653 & 396 \\ 30 & 86 & 300 & 378 & 396 & 962 \end{bmatrix}$
1	$\begin{Bmatrix} 3.2 \\ 3.3 \\ 4.1 \\ 2.5 \\ 2.4 \\ 3.0 \end{Bmatrix}$	$\begin{bmatrix} 0.11 & 0.67 & 0.54 & 0.18 & 0.08 & 0.53 \\ 0.03 & 0.55 & 0.24 & 0.18 & 0.80 & 0.19 \\ 0.02 & 0.73 & 0.06 & 0.53 & 0.66 & 0.75 \\ -0.01 & 0.22 & 0.89 & 0.85 & 0.99 & 0.75 \\ -0.01 & -0.61 & -0.32 & 0.82 & -0.14 & -0.30 \\ -0.02 & -0.32 & -0.46 & 0.81 & -0.67 & 0.68 \end{bmatrix}$	$\begin{Bmatrix} 0.11 \\ -0.06 \\ -0.06 \\ 0.01 \\ 0.13 \\ 0.02 \end{Bmatrix}$	6	$10^{-4}\times\begin{bmatrix} 6 & 2 & 5 & 5 & -7 & 3 \\ 2 & 15 & 16 & 7 & -22 & 8 \\ 4 & 16 & 66 & 49 & -41 & 94 \\ 6 & 8 & 49 & 288 & 17 & 108 \\ -2 & -18 & -37 & 18 & 294 & 19 \\ 8 & 11 & 94 & 108 & 19 & 820 \end{bmatrix}$
5	$\begin{Bmatrix} \text{Inf} \\ 176 \\ \text{Inf} \\ \text{Inf} \\ 450 \\ 641 \end{Bmatrix}$	$10^{-4}\times\begin{bmatrix} 185 & 113 & 93 \\ 5 & -11 & -10 \\ -18 & -6 & -5 \\ -1 & -1 & -1 \\ 2 & 1 & 1 \\ 1 & 1 & 0 \end{bmatrix}$	$\begin{Bmatrix} -0.32 \\ 0.02 \\ 0.08 \end{Bmatrix}$	3	$10^{-4}\times\begin{bmatrix} 3 & 2 & 5 & 4 & -8 & 2 \\ 2 & 16 & 17 & 5 & -25 & 7 \\ 5 & 17 & 67 & 49 & -43 & 93 \\ 4 & 5 & 49 & 293 & 16 & 118 \\ -8 & -25 & -43 & 16 & 302 & 20 \\ 3 & 7 & 93 & 118 & 20 & 823 \end{bmatrix}$
9	$\begin{Bmatrix} \text{Inf} \\ 798 \\ \text{Inf} \\ \text{Inf} \\ \text{Inf} \\ \text{Inf} \end{Bmatrix}$	$10^{-4}\times\begin{bmatrix} 270 \\ 18 \\ -29 \\ -1 \\ 4 \\ 2 \end{bmatrix}$	$\{-0.18\}$	1	$10^{-4}\times\begin{bmatrix} 2 & 3 & 6 & 5 & -8 & 3 \\ 3 & 17 & 18 & 6 & -25 & 7 \\ 6 & 18 & 68 & 49 & -43 & 93 \\ 5 & 6 & 49 & 299 & 16 & 120 \\ -8 & -25 & -43 & 16 & 302 & 21 \\ 3 & 7 & 93 & 120 & 21 & 835 \end{bmatrix}$

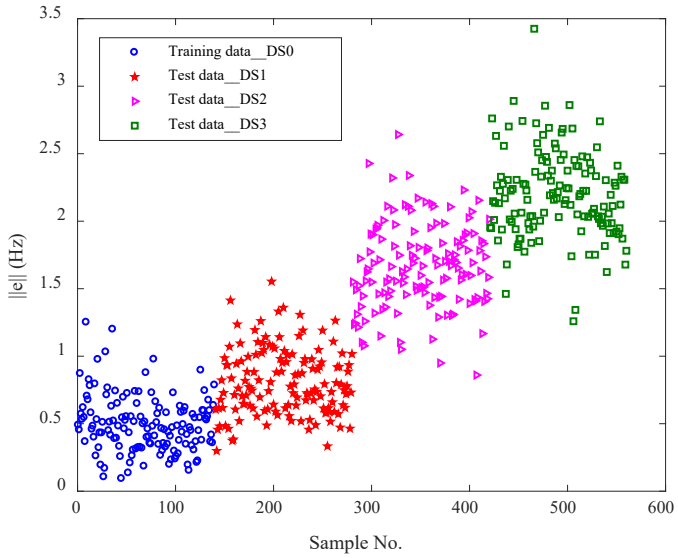

Figure 7 Residue of reconstruction using the first six frequencies

In practical modal testing, higher frequency modes are difficult to measure. We therefore pretend that the sixth mode was not measured in all the DSs and only the first five modes are used for damage detection. The proposed FA technique is repeated and the resulting residues are plotted in Figure 8. Reconstruction errors of test data in DS1 have no noticeable difference with those of DS0 after removing mode 6. This result implies that mode 6 is more sensitive to the slight damage compared with the first five modes. Thus, when only the first five modes are used in DS1, a false-negative damage diagnosis happens where DS1 is falsely recognized as undamaged. In this situation, data collected in DS1 may be falsely used as the training data. Suppose that the first five modes collected in DS0 and DS1 are both used as training data. Variations of the latent variable and parameters are shown in Table 4. The number of columns of $\mathbf{W}$ converges to one after eleven iterations, and the number of latent factors in $\mathbf{z}_n$ is also one, as in Table 3. The errors in all DSs are calculated and plotted in Figure 9. Significant deviations are observed between the training data (DS0 and DS1) and test data (DS2 and DS3). The results indicate that although the slight damage was falsely identified as undamaged at the beginning, the proposed method is still capable of detecting damage correctly at later stages where damage severity increases.

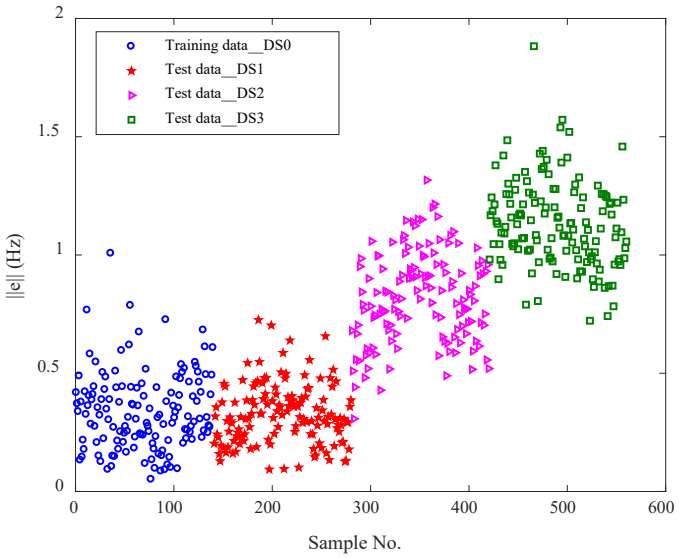

Figure 8 Reconstruction error using the first five frequencies

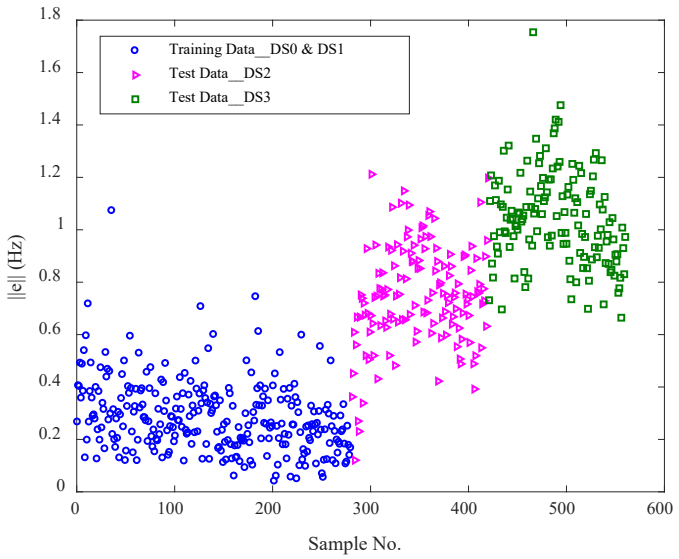

Figure 9 Reconstruction error using DS0 & DS1 as training data

Table 4 Variations of the variable and parameters using DS0 & DS1 as training data

No.	α	$\mathbf{W}$	$\mathbf{z}_1$	M	$\mathbf{\Psi}$
0		$\begin{bmatrix} 0.37 & 0.03 & 0.88 & 0.32 & 0.38 \\ 0.58 & 0.01 & 0.44 & 0.55 & 0.86 \\ 0.15 & 0.80 & 0.09 & 0.48 & 0.69 \\ 0.10 & 0.68 & 0.63 & 0.42 & 0.51 \\ 0.75 & 0.77 & 0.11 & 0.80 & 0.42 \end{bmatrix}$		5	$10^{-3} \times \begin{bmatrix} 4 & 5 & 19 & 24 & 25 \\ 5 & 31 & 54 & 68 & 71 \\ 19 & 54 & 373 & 235 & 247 \\ 24 & 68 & 235 & 593 & 311 \\ 25 & 71 & 247 & 311 & 653 \end{bmatrix}$

11	$\begin{Bmatrix} \text{Inf} \\ 1561 \\ \text{Inf} \\ \text{Inf} \\ \text{Inf} \end{Bmatrix}$	$10^{-4}\times\begin{bmatrix} 177 \\ -23 \\ -6 \\ -2 \\ 2 \end{bmatrix}$	$\{-0.11\}$	1	$10^{-4}\times\begin{bmatrix} 2 & 5 & 7 & 6 & 1 \\ 5 & 30 & 36 & 18 & 18 \\ 7 & 36 & 77 & 51 & 23 \\ 6 & 18 & 51 & 181 & 37 \\ 1 & 18 & 23 & 37 & 204 \end{bmatrix}$

6. Conclusions

A sparse Bayesian FA-based method for output-only structural damage detection without measuring the varying environmental parameters is developed in this study. The number of underlying environmental factors is automatically identified by adopting the ARD prior in the SBL framework. The reconstruction error is then calculated as the damage indicator according to the generative FA model. The proposed method is applied to two experimental examples under varying environmental conditions. The RC slab example demonstrates that the sparse Bayesian FA-based method can automatically identify the number of significant environmental factors that influence structural dynamic properties. The steel frame example shows that the proposed method can successfully detect the existence of damage. The measurement of the varying environmental factors is unnecessary in both examples.

Acknowledgements

The research in this paper was supported by the Key-Area Research and Development Program of Guangdong Province (Project No. 2019B111106001), RGC-GRF (Project No. 15201920) and PolyU Project of Strategic Importance (Project No. 1-ZE1F).

References

1. C.R. Farrar, S.W. Doebling, D.A. Nix, Vibration-based structural damage identification, Philosophical Transactions of the Royal Society of London. Series A: Mathematical, Physical and Engineering Sciences, 359 (2001) 131–149.

2. W. Fan, P.Z. Qiao, Vibration-based damage identification methods: a review and comparative study, Structural Health Monitoring, 10 (2011) 83–111.

3. R.R. Hou, Y. Xia, Review on the new development of vibration-based damage identification for civil engineering structures: 2010–2019, Journal of Sound and Vibration, under review.

4. J. Zhang, Y.L. Xu, Y. Xia, J. Li, A new statistical moment-based structural damage detection method, Structural Engineering and Mechanics, 30 (2008) 445–466.

5. Y. Huang, C.S. Shao, B.A. Wu, J.L. Beck, H. Li, State-of-the-art review on Bayesian inference in structural system identification and damage assessment, Advances in Structural Engineering, 22 (2019) 1329–1351.

6. H. Sohn, M. Dzwonczyk, E.G. Straser, A.S. Kiremidjian, K.H. Law, T. Meng, An experimental study of temperature effect on modal parameters of the Alamosa Canyon Bridge, Earthquake Engineering and Structural Dynamics, 28 (1999) 879–897.

7. B. Peeters, G. De Roeck, One-year monitoring of the Z24-Bridge: environmental effects versus damage events, Earthquake Engineering and Structural Dynamics, 30 (2001) 149–171.

8. Y. Xia, H. Hao, G. Zanardo, A. Deeks, Long term vibration monitoring of an RC slab: Temperature and humidity effect, Engineering Structures, 28 (2006) 441–452.

9. C.Y. Liu, J.T. DeWolf, Effect of temperature on modal variability of a curved concrete bridge under ambient loads, Journal of Structural Engineering, 133 (2007) 1742–1751.

10. Q.W. Zhang, L.C. Fan, W.C. Yuan, Traffic-induced variability in dynamic properties of cable-stayed bridge, Earthquake Engineering and Structural Dynamics, 31 (2002) 2015–2021.

11. Siringoringo DM, Fujino Y, System identification of suspension bridge from

ambient vibration response, Engineering Structures, 30 (2008) 462–477.

12. A. Cunha, E. Caetano, F. Magalhaes, C. Moutinho, Recent perspectives in dynamic testing and monitoring of bridges, Structural Control and Health Monitoring, 20 (2013) 853–877.

13. Y.L. Ding, A.Q. Li, Temperature-induced variations of measured modal frequencies of steel box girder for a long-span suspension bridge, International Journal of Steel Structures, 11 (2011) 145–155.

14. Y. Bao, Y. Xia, H. Li, Y.L. Xu, P. Zhang, Data fusion-based structural damage detection under varying temperature conditions, International Journal of Structural Stability and Dynamics, 12 (2012).

15. B. Moaveni, I. Behmanesh, Effects of changing ambient temperature on finite element model updating of the Dowling Hall Footbridge, Engineering Structures, 43 (2012) 58–68.

16. R.R. Hou, X.Y. Wang, Q. Xia, Y. Xia, Sparse Bayesian learning for structural damage detection under varying temperature conditions, Mechanical Systems and Signal Processing, 145(2020): 106965.

17. H. Sohn, K. Worden, C.R. Farrar, Novelty detection under changing environmental conditions, International Society for Optics and Photonics, 4330 (2001) 108–118.

18. H.F. Zhou, Y.Q. Ni, J.M. Ko, Structural damage alarming using auto-associative neural network technique: Exploration of environment-tolerant capacity and setup of alarming threshold, Mechanical Systems and Signal Processing, 25 (2011) 1508–1526.

19. E. Figueiredo, G. Park, C.R. Farrar, K. Worden, J. Figueiras, Machine learning algorithms for damage detection under operational and environmental variability, Structural Health Monitoring, 10 (2011) 559–572.

20. T.Y. Hsu, C.H. Loh, Damage detection accommodating nonlinear environmental effects by nonlinear principal component analysis, Structural Control and Health Monitoring, 17 (2010) 338–354.

21. A.M. Yan, G. Kerschen, P. De Boe, J.C. Golinval, Structural damage diagnosis under varying environmental conditions - Part I: A linear analysis, Mechanical Systems and Signal Processing, 19 (2005) 847–864.

22. A.M. Yan, G. Kerschen, P. De Boe, J.C. Golinval, Structural damage diagnosis under varying environmental conditions - part II: local PCA for non-linear cases, Mechanical Systems and Signal Processing, 19 (2005) 865–880.

23. A. Deraemaeker, E. Reynders, G. De Roeck, J. Kullaa, Vibration-based structural health monitoring using output-only measurements under changing environment, Mechanical Systems and Signal Processing, 22 (2008) 34–56.

24. A. Deraemaeker, K. Worden, A comparison of linear approaches to filter out environmental effects in structural health monitoring, Mechanical Systems and Signal Processing,105 (2018) 1–15.

25. J. Kullaa, Distinguishing between sensor fault, structural damage, and environmental or operational effects in structural health monitoring, Mechanical Systems and Signal Processing, 25 (2011) 2976–2989.

26. Y.Q. Ni, X.G. Hua, K.Q. Fan, J.M. Ko, Correlating modal properties with temperature using long-term monitoring data and support vector machine technique, Engineering Structures, 27(2005) 1762–1773.

27. J. Kullaa, Structural health monitoring under nonlinear environmental or operational influences, Shock and Vibration, 2014 (2014).

28. E. Reynders, G. Wursten, G. De Roeck, Output-only structural health monitoring in changing environmental conditions by means of nonlinear system identification, Structural Health Monitoring, 13 (2014) 82–93.

29. D. Sen, K. Erazo, W. Zhang, S. Nagarajaiah, L.M. Sun, On the effectiveness of principal component analysis for decoupling structural damage and environmental effects in bridge structures, Journal of Sound and Vibration, 457 (2019) 280–298.

30. H. Li, S.L. Li, J.P. Ou, H.W. Li, Modal identification of bridges under varying environmental conditions: Temperature and wind effects, Structural Control and Health Monitoring, 17 (2010) 495–512.

31. C.M. Bishop, Pattern Recognition and Machine Learning, Springer, Berlin, 2006.

32. J.L. Beck, K.V. Yuen, Model selection using response measurements: Bayesian probabilistic approach, Journal of Engineering Mechanics, 130 (2004) 192–203.

33. R. Sandhu, C. Pettit, M. Khalil, D. Poirel, A. Sarkar, Bayesian model selection using automatic relevance determination for nonlinear dynamical systems,

Computer Methods in Applied Mechanics and Engineering, 320 (2017) 237–260.

34. F. Qian, W. Zheng, An evolutionary nested sampling algorithm for Bayesian model updating and model selection using modal measurement, Engineering Structures, 140 (2017) 298–307.

35. J. Piironen, A. Vehtari, Comparison of Bayesian predictive methods for model selection, Statistics and Computing, 27 (2017) 711–735.

36. Z.H. Ding, J. Li, H. Hao, Structural damage identification using improved Jaya algorithm based on sparse regularization and Bayesian inference, Mechanical Systems and Signal Processing, 132 (2019) 211–231.

37. H.F. Lam, J.H. Yang, S.K. Au, Markov chain Monte Carlo-based Bayesian method for structural model updating and damage detection, Structural Control and Health Monitoring, 25 (2018) e2140.

38. W.J. Yan, L.S. Katafygiotis, A two-stage fast Bayesian spectral density approach for ambient modal analysis. Part I: Posterior most probable value and uncertainty, Mechanical Systems and Signal Processing, 54-55 (2015) 139–155.

39. J.L. Beck, Bayesian system identification based on probability logic, Structural Control and Health Monitoring, 17 (2010) 825–847.

40. X.Y. Wang, R.R. Hou, Y. Xia, X.Q. Zhou, Structural damage detection based on variational Bayesian inference and delayed rejection adaptive Metropolis algorithm, Structural Health Monitoring, (2020).

41. M.E. Tipping, Sparse Bayesian learning and the relevance vector machine, Journal of Machine Learning Research, 1 (2001) 211–244.

42. M.E. Tipping, C.M. Bishop, Probabilistic principal component analysis, Journal of the Royal Statistical Society: Series B (Statistical Methodology), 61 (1999) 611–622.

43. C.M. Bishop, Bayesian PCA, Advances in Neural Information Processing Systems 11, 11 (1999) 382–388.

44. D. J. Bartholomew, M. Knott, I. Moustaki, Latent Variable Models and Factor Analysis: A Unified Approach, John Wiley & Sons, 2011.

45. P. S. Laplace, Memoir on the probability of the causes of events, Statistical Science, 1(1986) 364–378.

46. J.L. Beck, L.S. Katafygiotis, Updating models and their uncertainties. I: Bayesian statistical framework, Journal of Engineering Mechanics, 124 (1998) 455–461.

47. J.L. Beck, Statistical system identification of structures, In Proceedings of International Conference on Structural Safety and Reliability, ASCE, 1989, pp. 1395–1402.

48. X.Y. Wang, R.R. Hou, Y. Xia, X.Q. Zhou, Laplace approximation in sparse Bayesian learning for structural damage detection, Mechanical Systems and Signal Processing, 140 (2020).